

In Situ Visualizing the Interplay Between the Separator and Potassium Dendrite Growth by Synchrotron X-ray Tomography

Ling Ni[†], Markus Osenberg[§], Haijun Liu[†], André Hilger[§], Libao Chen[‡], Dong Zhou[§], Kang Dong[§], Tobias Arlt[§], Xiayin Yao[§], Xiaogang Wang^{†,*}, Yanan Chen[#], Yutao Li[¶], Kangning Zhao^Δ, Chao Yang^{§,*}, Ingo Manke[§], Fu Sun^{†,*}, and Renjie Chen[‡]

[†]Qingdao Institute of Bioenergy and Bioprocess Technology, Chinese Academy of Sciences, Qingdao 266101, China

[§]Helmholtz Centre Berlin for Materials and Energy, Hahn-Meitner-Platz 1, Berlin 14109, Germany

[‡]State Key Laboratory for Powder Metallurgy, Central South University, Changsha 410083, China

[§]Ningbo Institute of Materials Technology & Engineering, Chinese Academy of Sciences, Ningbo 315201, China

[#]School of Materials Science and Engineering, Tianjin University, Tianjin 300350, China

[¶]Materials Science and Engineering Program and Texas Materials Institute, the University of Texas at Austin, Texas 78712, United States

^ΔLaboratory of Advanced Separations (LAS) École Polytechnique Fédérale de Lausanne (EPFL), Sion CH-1950, Switzerland

[‡]School of Materials Science & Engineering, Beijing Institute of Technology, Beijing, 100081, China

Corresponding Author

*E-mail: wangxg@qibebt.ac.cn (X. Wang), chao.yang@helmholtz-berlin.de (C. Yang), sunfu@qibebt.ac.cn (F. Sun)

ABSTRACT

Rechargeable potassium (K) batteries are a promising next-generation technology for low-cost grid scale energy storage applications. Nevertheless, the undesirable interfacial instabilities originating from the interplay between the employed separators and electrodes largely compromise the battery's performance, and the underlying mechanism of which remains elusive. Herein, the interfacial stability between three types of commercial separators (Celgard 2325, Celgard 2400 and GF/D) and the K electrodeposits is investigated in K|K symmetric cells via *in-situ* Synchrotron X-ray tomography technique. It is demonstrated that the cell built with a Celgard 2400 separator can achieve a stable cycling performance due to its high mechanical strength

and integrity along the thickness direction, thus alleviating the K dendrites growth. In contrast, a GF/D membrane of low mechanical cohesion and excessive porosity is found to be easily deformed and filled with deciduous potassium dendritic aggregates during battery cycling. Similarly, the tri-layer Celgard 2325 separators, which are weakly bonded by interlaminar forces, are found to be severely delaminated by the overgrowth of K dendrites. Furthermore, it is revealed that the delamination failure behaviors of Celgard 2325 is driven by the local stress induced by the spatially and heterogeneously formed "dead" K dendrites. Our work provides direct visualization of morphological evolvement of the separators in presence of potassium dendrites in K|K symmetric cells.

Introduction

With the soaring energy storage requirement for intermittent solar and wind energy, developing high energy-density lithium-ion batteries (LIBs) is a vital choice.¹ However, LIBs cannot meet the demand for low-cost and large-scale energy storage because of the lithium rarity (0.0017 wt%) and uneven distribution.² Potassium-based rechargeable batteries are gaining rapid scientific attention as promising alternative for the upcoming stationary and electrical grid applications, due to the abundant resources and low potential of K.^{3,4} In addition, K^+ also possesses a higher transference number and ionic conductivity than that of Na^+ and Li^+ due to its low desolvation energy and weak Lewis acidity, which is beneficial to facilitate fast diffusion kinetics during battery operation. such as potassium metal batteries (KMBs), potassium superoxide (K-O₂) and potassium-sulfur batteries (K-S).^{5,6} Wu *et al.* demonstrated that the K-O₂ battery based on thermodynamically and kinetically stable KO₂ can offer a high theoretical specific

1 energy density of 935 Wh kg⁻¹ under long-term cycling conditions.⁷ Chen *et al.*
2 demonstrated that the theoretical capacity of the potassium-sulfur battery could reach
3 1023 Wh kg⁻¹.⁸ The K metal batteries coupled with the conversion chemistry electrodes
4 (sulfur or oxygen cathodes) could deliver much higher energy densities than that of
5 LIBs, which is practically attractive for grid-scale energy storage applications.⁹

6 Although these studies have showcased the potential capabilities of KMBs, their
7 further development has been greatly hindered by many challenges, especially the
8 uncontrollable growth of K dendrites.¹⁰ Tremendous efforts have been proposed to
9 tackle the uncontrolled K dendrites by altering the solvents, designing artificial solid
10 electrolyte interphases (SEIs), using solid-state electrolytes, adding electrolyte
11 additives and constructing three dimensional (3D) host materials.¹¹⁻¹⁴ These endeavors
12 have contributed to the development of KMBs by alleviating the formation of K
13 dendrites to some extent during battery cycling. Nevertheless, reports of KMBs
14 possessing long-term cyclability under practical cycling conditions remain scarce.
15 Aiming to further improve their performance, an in-depth understanding of the
16 working/decaying mechanisms of KMBs are highly desirable.

17 From the battery's components point of view, separators play a pivotal role in
18 determining the cell performances during battery operation. In KMBs, the porous
19 separator together with its interaction with electrode materials and liquid electrolytes
20 (LEs), significantly affect the ion transport process and electrodeposition behavior of
21 K. The extensively used separators in rechargeable K batteries are the commercial
22 polyolefin separators and/or glass fiber (GF) membranes.¹⁶ These separators have been

1 widely used in LIBs and various strategies have been developed to further improve their
2 performance, among which includes the mechanical and physical enhancement,
3 together with the modification and functionality. These are the most practical and facile
4 methods to improve the mechanical/thermal properties of the commercial separators.¹⁷⁻
5 ¹⁹ Additionally, different properties of battery components in KMBs, including the
6 mechanical properties of K dendrites, the volume change behavior of K electrodes, the
7 solubility of decomposition products and SEI layers may exert dissimilar influence on
8 separators as that in LMBs.^{5,20,21} In fact, the interaction/interplay between K dendrites
9 growth and separators under realistic electrochemical conditions have been
10 insufficiently studied.

11 Herein, the exploration of the interaction between K electrodeposits and separators
12 is elaborately investigated based on the *in-situ* synchrotron X-ray tomography
13 technique (SX-CT) in K|K symmetric cells built with three commercial separators
14 (Celgard 2325, 2400, and GF/D). The high-resolution X-ray imaging could reveal the
15 underlying correlation between the electrochemical performance of the battery and the
16 battery components' change in a nondestructive way, it has been found that the large
17 pore size (micron scale) across the glass fiber separators can be easily filled with
18 dendritic K electrodeposits. It is also revealed that the multilayered Celgard 2325
19 separators can be delaminated into three layers by deciduous K dendrites due to the
20 mechanical stresses generated from the inhomogeneous formation of K deposition
21 during K plating/stripping, as confirmed by finite element method (FEM) analysis.
22 Compared to Celgard 2325 and GF/D separators, Celgard 2400 separators, which

feature strong mechanical properties and suitable thickness, are found to maintain high structural integrity and suppress the growth of K dendrites. This work affords the fundamental understanding of the interaction between K electrodeposits and the used separators and sheds new lights on developing rational strategies for high-performance separators for KMBs.

Results and Discussion

The composition and structure of the employed separators (Celgard 2325, 2400, and GF/D) are analyzed and the results are shown in Fig.1. The Scanning Electron Microscope (SEM) characterizations of the Celgard separators, as shown in Fig. 1a,b, obviously show the highly oriented "slit-like" pore structures parallel to the stretching direction (uniaxial stretching direction).²⁶ Notably, the pore size of Celgard 2400 separators are much larger than those of Celgard 2325 separators, as confirmed by Barrett–Joyner–Halenda (BJH) (Fig. 1c). Cross-sectional SEM images of both the membranes (Fig. 1d, e) clearly show that the Celgard 2325 separator is a membrane composed of tri-layers (polypropylene-polyethylene-polypropylene (PP|PE|PP)), while Celgard 2400 separator is assembled by bilayer PP membranes.^{27,28} The amplified images (insets of Fig. 1d, e) not only demonstrate the existence of an interlayer spacing among the composing layers but also confirm that the thickness of each layer of Celgard 2325 (~8 μm) was less than that of Celgard 2400 (~12 μm). The X-ray diffraction (XRD) measurement in Fig. S1 further corroborates the composition of these multilayer separators.²⁶ Fig.1f presents the SEM result of the GF/D separator, which is formed by the typical nonwoven glass fibers under low mechanical cohesion state.²⁹

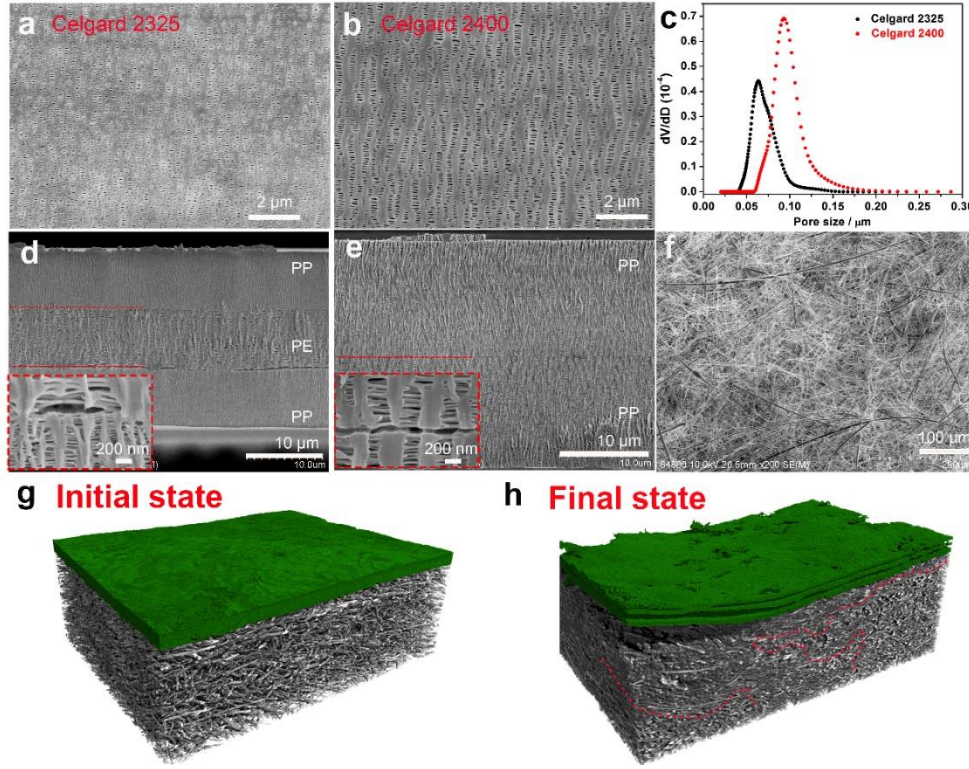


Fig. 1. (a)-(e) The surface SEM images, BJH desorption pore-size distribution and cross-sections of Celgard 2325 and Celgard 2400 separators, respectively. The insets of (d), (e) are the enlarged interface spacing between composing layers. (f) The surface SEM image of GF/D separator. (g) 3D rendered volume of a pristine Celgard 2325 and GF/D immersed into electrolyte 1 M KTFSI within a K|K symmetric cell. (h) 3D rendered volume of the Celgard 2325 and GF/D within a K|K symmetric cell after discharging at 0.5 mA cm^{-2} .

The evolution of the interphase between the separator and K electrodes as well as the morphological evolution of the electrodeposited K in symmetric K|K cells are visualized by *in-situ* Synchrotron X-ray computed tomography (SX-CT). A total number of 7 cells built with different electrolytes (1M KTFSI (EC/DEC (v/v) =1:1), 0.8 M KPF6 (EC/DEC (v/v) =1:1 and 1M KFSI (EC/DEC (v/v) =1:1)) and cycled under different conditions are studied. The detailed information of these studied cells is concisely shown in Table 1. Fig. S2 shows the schematic *in-situ* measurement setup

and the corresponding measuring protocols, in which, the customized tomography cell (tomo-cell) is rotated 180° while 2400 projections of 25 milliseconds exposure time are collected. The spatial resolution of 1.2 μm is achieved by using the 10X objective system and a 2 by 2 binning process. The specific battery assembly procedures, SX-CT measurement parameters, and tomography data analysis could be found in the Methods Section in Supporting Information (SI). The 3D rendering of the uncycled cell *No.1* is shown in Fig. 1g, from which the Celgard 2325 separator (green) and the GF/D separator (black) are found to maintain their original compact structure. A SX-CT scan of cell *No.2* after discharging for 67 h (Fig. S4) is conducted to investigate the change of Celgard 2325 and the results are shown in Fig. 1h. It vividly demonstrates that the originally integrated Celgard 2325 is delaminated into three layers and the pore spaces of GF/D is filled with a large amount of K dendrites (red dot line). The increase of voltage polarization of the *No.2* cell (Fig. S4) is in accordance with the accumulated K electrodeposits in which insulating SEI layers would be continuously generated due to the formation of new surfaces during the electrodeposition process.³⁰

Table 1 The details of the studied cells in the current experiment

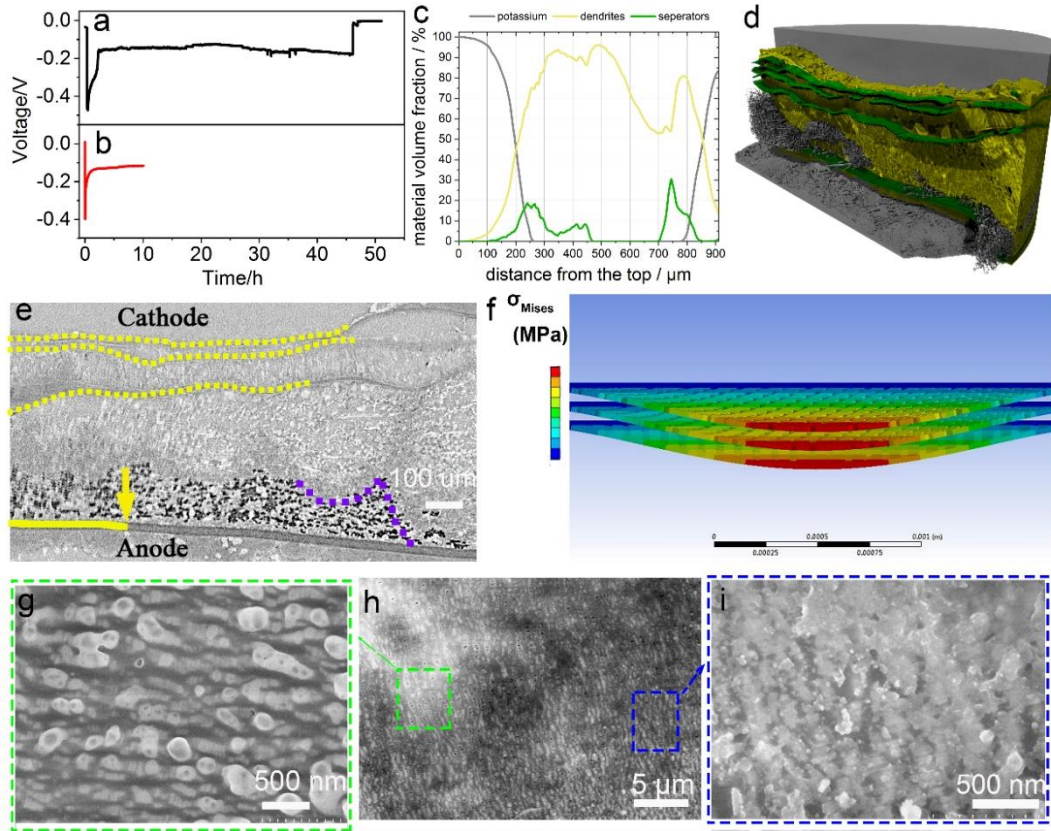
Cell <i>No.</i>	Electrolyte	Current density (mA cm ⁻²)	Duration time (h)	Separator	Measurement protocole	Cell structure
1	1 M KTFSI (EC/DEC (v/v) =1:1)		0	Celgard 2325+GF/D+ Celgard 2325	Standing	Tomo- cell
2	1 M KTFSI (EC/DEC (v/v) =1:1)	0.5	67	Celgard 2325+GF/D+ Celgard 2325	Discharge	Tomo- cell
3	0.8 M KPF ₆ (EC/DEC (v/v)	0.5	46	Celgard 2325+GF/D+	Discharge	Tomo- cell

	=1:1)			Celgard 2325		
4	0.8 M KPF ₆ (EC/DEC (v/v) =1:1)	0.5	10	Celgard 2325+GF/D+	Discharge	coin cell
	=1:1)			Celgard 2325		
5	1 M KFSI (EC/DEC (v/v) =1:1)	0.5/1h	116	Celgard 2325+GF/D+	Cycle	Tomo- cell
	=1:1)			Celgard 2325		
6	1 M KFSI (EC/DEC (v/v) =1:1)	2/0.5h	118	Celgard 2325+GF/D+	Cycle	Tomo- cell
	=1:1)			Celgard 2325		
7	1 M KFSI (EC/DEC (v/v) =1:1)	0.5/1h	160	Celgard 2400+GF/D+	Cycle	Tomo- cell
	=1:1)			Celgard 2400		

Dendrite growth phenomena have been frequently observed during alkali metal anodes electrodeposition while their specific morphologies vary with electrolyte components, the depth of discharge, current densities, cycling conditions and separator.³¹ Using Celgard 2325 and GF/D separators, different types of electrolytes and varied depth of cycling conditions are studied in terms of their abilities to "stop" the growth of K dendrites towards the separators. Using 1 M KPF₆-EC/DEC electrolytes, the cell No.3 tested in Fig. 2a was short-circuited after 45 h. The short-circuited failure mechanism may result from the continuously accumulated K dendrites easily propagating through the membrane. From the *in-situ* SX-CT images (Fig. 2e), K dendrites are found to approach toward the counter electrode (yellow solid line in Fig. 2e), which is consistent with the cell's electrochemical performance. Moreover, one can observe that the Celgard 2325 contacting K cathode (defined as cathode because it experiences electrodeposition) is delaminated into three layers (between yellow dash lines) by K dendrites and the pores space of GF/D (between yellow dash line and solid line) are filled with deciduous K electrodeposit aggregates. These observations are in

1 a stark contrast with that of the Celgard 2325 separator nearby K anode (solid yellow
2 line). The segmented tomography data (Fig. 2c) of the spatial distribution of K dendrites,
3 together with the corresponding integral 3D rendering (Fig. 2d), demonstrate that a
4 large number of K electrodeposits have permeated through the Celgard 2325 separator
5 and then accumulated inside the loose compartments of the GF/D separator. In addition,
6 the finite element analysis (FEA) is undertaken to simulate the distribution of
7 equivalent (Von-Mises) stress generated due to the dynamic volume expansion of K
8 electrodeposits as well as the stress evolution exerted on the neighbouring Celgard
9 2325.³² From this simulation (Fig. 2f), it is hypothesized that the delamination of
10 Celgard 2325 is driven by the locally inhomogeneous pressure generated from K
11 electrodeposits, *e.g.*, the K dendrites. This agrees well with the observation that K
12 dendrites tend to penetrate through the pores and stratify the multilayer separators,
13 followed by continuous propagation/migration towards the GF/D separator. To further
14 understand the dynamic propagation/migration process of the K electrodeposits inside
15 the Celgard 2325 separator, short-time discharge test (cell *No.*4) was conducted (Fig.
16 2b). Because cell *No.*4 was discharged for 5 h, one would expect that the amount of K
17 electrodeposits is less and some electrodeposits may grow through the pores of the
18 separator. This scenario is confirmed by SEM measurement and the results are vividly
19 shown in Fig. 2g, h, and i, from which the penetration/trespass of K electrodeposits
20 through the pores of the separator is unambiguously notable (Fig. 2g). A closer
21 examination further suggests that the pores' size become smaller due to K dendrites
22 blocking (Fig. 2h). In certain areas (blue dash box), it is found that some of the K

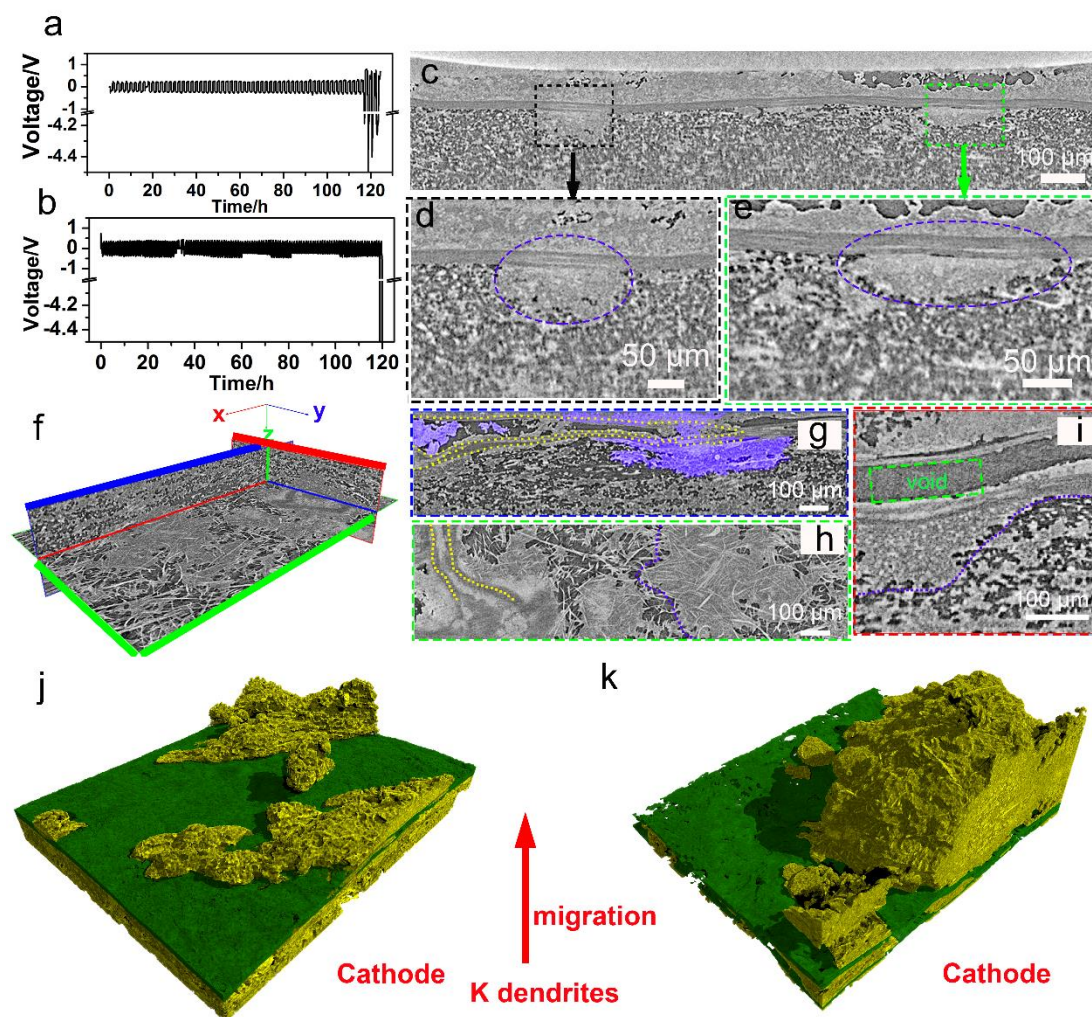
1 dendrites are agglomerated on the surface of separators (Fig. 2i) after they have “grow”
 2 through them. To conclude, these results suggest that K electrodeposits can penetrate
 3 easily through the pores of Celgard 2325 separator and continue to grow through the
 4 glass fiber membrane.³³



6 Fig. 2. The electrochemical performance and morphological evolution of Celgard 2325 within K|K
 7 symmetric cells (using 0.8 M KPF₆ in EC/DEC (v/v)=1:1 electrolyte). (a), (b) The discharge curves
 8 of cell No. 3 and 4, respectively. (c) The volume fraction of K deposition in d) along the through-
 9 plane direction from cathode K to the anode K. (d) 3D reconstructed volumes of cell No. 3. (e)
 10 Cross-sectional view of slice from cell No. 3. (f) Simulation of compression stress of regions where
 11 K deposition contacted with the Celgard 2325.³² (h) The SEM image of Celgard 2325 separator
 12 harvested from cell No. 4. (g), (i) The enlargement of SEM images in green and blue dash box of
 13 Fig. h.

1 The experiment and simulation shown above provide important insights into how
2 the Celgard 2325 can be delaminated into three layers by the continuously growing K
3 electrodeposits, *e.g.*, dendrites, whiskers and/or filaments, during discharge process.
4 Practically speaking, understanding the interactions between the separator and the K
5 electrodeposits under extended cycling condition is highly desirable. For this reason,
6 two more cells (*No.* 5, and 6) are electrochemically cycled before the SX-CT
7 measurement and their voltage profiles are shown in Fig. 3a, b. The increased voltage
8 overpotential of these two cells suggest that their failure is caused by a steady increase
9 of cell impedance, which agrees well with their electrochemical impedance spectrum
10 (EIS) results (Fig. S5a, b).^{34,35} The SX-CT results of these two cells are shown in Fig.
11 3c-k. As shown in the cross-sectional slice of cell *No.*5 (Fig. 3c), one can observe that
12 a highly porous and loose K electrodeposits structure, with parts of them disconnected
13 from the current collector and forming "dead" K (Fig. 3c), is generated after
14 electrochemical cycling. The enlarged images (Fig. 3d, e) provide direct visual
15 evidence of the penetration of K electrodeposits through the Celgard 2325 separator, as
16 well as an inhomogeneous distribution of K electrodeposits during battery operation. In
17 addition, one can clearly note that the Celgard 2325 separator is stratified into three
18 layers within local regions (Fig. 3d, e, purple dash lines). Fig.3f shows an orthorhombic
19 slice view of the internal state of cell *No.*6 and the corresponding slices (along x, y, and
20 z-direction) are individually shown in Fig.3g, h, and i. It can be observed from Fig. 3g
21 that the K electrode becomes porous after electrochemical cycling and some of the K-
22 metal domains are electrically disconnected from the current collector, resulting in

1 severe migration of "dead" K (purple area) and void space.³³ The delamination behavior
 2 of the Celgard 2325 separator is also obvious in cell No. 6 (Fig.3 g, h, yellow dot lines).
 3 The K dendrites migration/propagation becomes more severe with increased areal
 4 current density, as confirmed from the 3D renderings of cell No.5 and No.6 (Fig. 3j, k).
 5 The vigorous propagation/migration behavior of K electrodeposits may be related to
 6 their penetrability of different composing components, such as moss-like, tree-like
 7 and/or needle-like features.³⁶ These observations directly demonstrate that the physical
 8 deformation behavior of separators can be significantly influenced by the test mode,
 9 e.g., the current density and the electrodeposits morphologies.



10
 11 Fig. 3. Electrochemical data and mechanical degradation of Celgard 2325 and GF/D in cell No.5

1 and cell *No.6*. (a), (b) Galvanostatic cycling curves of cell *No.5* and *No.6*. (c) 2D SX-CT cross-
2 sectional slice of cell *No.5*. (d), (e) the enlarged images of the delaminated separator and blocked
3 GF by the accumulated "dead" K in black and green boxes in (c). (f), (g), (h), and (i) represent
4 orthogonal slices and the cross-sectional slices with xz, xy, yz face of the cell *No.6*. (j), (k) 3D
5 reconstructed volumes of cell *No.5* and *No.6*, respectively.

6
7 It is worthy to note that the delamination failure behavior of Celgard 2325 in
8 KMBs is inherently different from the fracture and melting behavior in lithium metal
9 battery (LMB).³⁷ One may attribute the difference to the high Young's modulus of Li
10 whiskers, up to 130 MPa, that greatly exceeds the Young's modulus of the
11 separator.^{38,39} In addition, the shear modulus of potassium metal (1.3 GPa) is also lower
12 than that of lithium metal (4.1 GPa), which is potentially another explanation.^{5,40} The
13 lamination of Celgard 2325 separator indicates that the weak interaction force among
14 the PP/PE/PP layers could not sustain the dramatic volume change of K-nearly 4 times
15 larger than that of Li-during potassium plating/stripping process. Nevertheless, it has to
16 be noted that the mechanical integrity of the separators is mainly related to the
17 manufacturing process using winding machines to laminate the three independent
18 layers into one single separator by mechanical compression.³⁷ Based on the previous
19 knowledge, the growth of K dendritic structures may be more easily alleviated by
20 employing separators of higher mechanical stability.⁴¹⁻⁴³

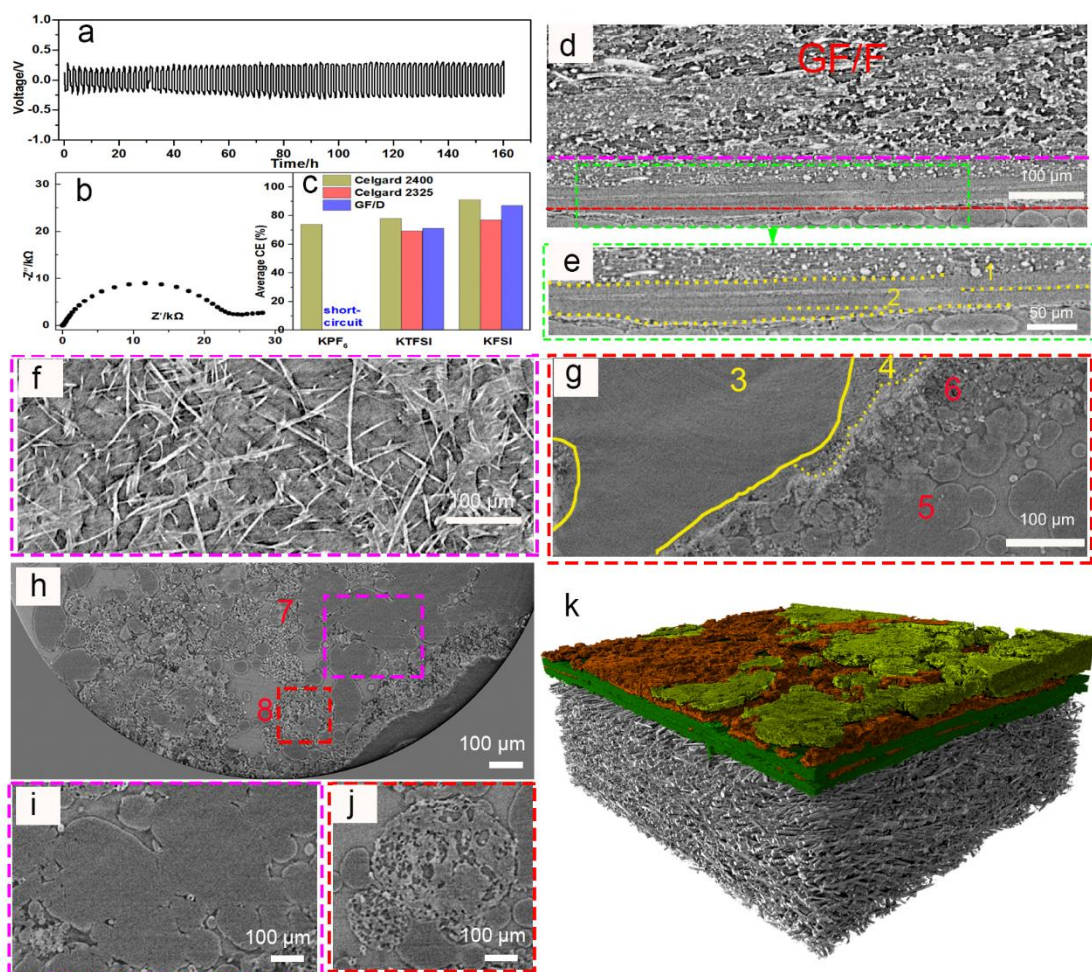


Fig. 4. The electrochemical data and morphology of K electrodeposits in cell No.7. (a), (b) Galvanostatic cycling curve and electrochemical impedance spectrum of cell No.7 after discharge for 160 h. (c). (d) 2D cross-sectional slice of cell No.7. (e) The enlarged image of the green dash box in Fig. 4c. (f), (g) Horizontal slices corresponding to the pink and red dash line in Fig. 4c. (h) Horizontal slice of deposited K close to the Celgard 2400 separator. (i), (j) The enlarged images of deposited K in the pink (7) and red (8) dash box of Fig. 4g. (k) 3D rendering of cell No.7, the yellow and brick-red regions represent bulky K depositions, and porous structure, respectively.

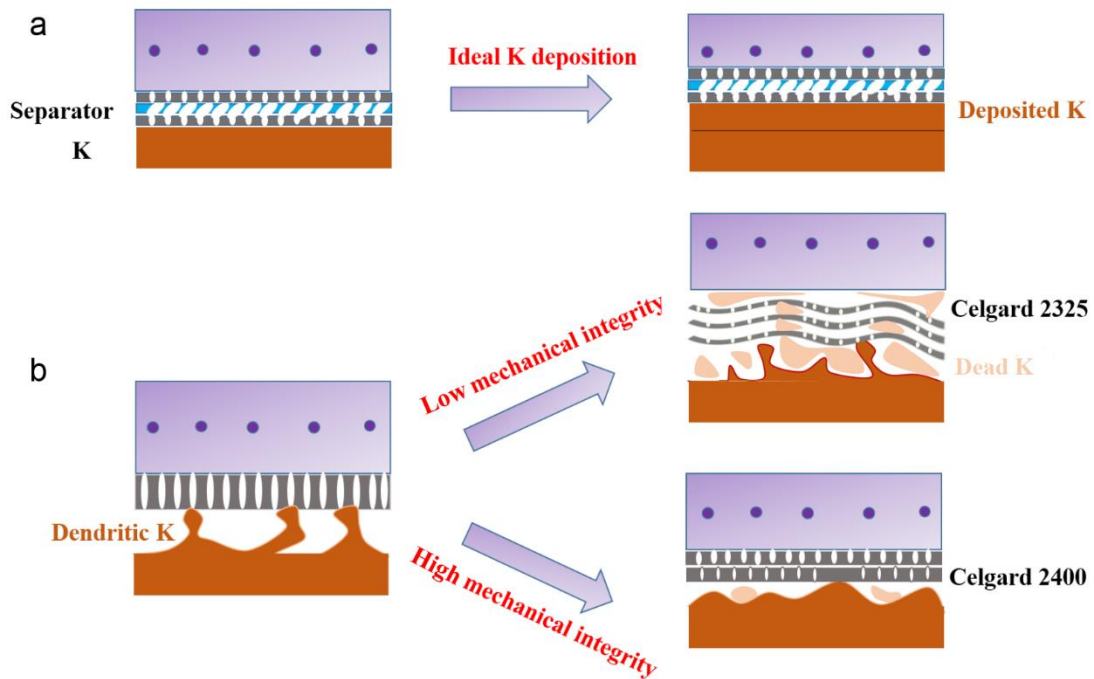
Compared with Celgard 2325 separators, Celgard 2400 separators, which are consisted of two thick-layers membrane of polypropylene (PP), possess relatively higher mechanical integrity.^{44,45} To probe the mechanical effect of Celgard 2400 on the electrochemical deposition/dissolution behavior of K, galvanostatic cycling of

1 symmetric cell (*No.7*) built with Celgard 2400 at 0.5 mA cm^{-2} is conducted and the
2 results are shown in Fig.4. As shown in Fig. 4a, the cell displays stable voltage
3 hysteresis without obvious fluctuations over the course of a 160 h experiment. The
4 smooth and flat voltage profile suggests that the Celgard 2400 separator can ensure a
5 homogeneous K deposition/dissolution. The EIS (Fig. 4b) result reveals a much smaller
6 interfacial resistance of the symmetrical K|K cell built using the Celgard 2400 separator
7 compared with that using Celgard 2325 (Fig. S5). The SX-CT results shown in Fig.4d-
8 k provide extra insights into the improved electrochemical performance of cell *No.7*,
9 together with the experimental evidence that the morphology of K electrodeposits can
10 be tuned by using separators of high mechanical property. As shown in Fig. 4d and e,
11 it can be observed that the Celgard 2400 separator is slightly delaminated into two flat
12 PP sheets by the insertion of a small amount of electrodeposited K (yellow dash lines 1
13 and 2). The location where electrodeposited K could insert into the two PP layers may
14 be an engineered artifact of binding two thick PP layers during the manufacturing
15 process,⁴⁶ which agrees well with the SEM image of Fig. 1e. The morphological
16 changes of Celgard 2400 are further shown in area 2 of Fig. 4e and area 4 of Fig. 4g
17 (in-plan image corresponding to the red dash line in Fig.4d), from which one could
18 observe that the dense PP layer (region 3 of Fig. 4g) became loosened. The in-plane
19 image of GF/D (Fig.4f, corresponding to the pink dash line in Fig.4d) nearby Celgard
20 2400 shows no K dendrites aggregating. This indicates that the Celgard 2400 separator
21 is favorable to prevent the growth of dendritic K electrodeposits and penetration due to
22 its thick nature and enhanced mechanical structure. In addition, as shown in Fig. 4g

1 (area 5), cycled K metal displays a flat and bulky morphology with a small amount of
2 foam-like K (area 6 of Fig. 4g). Observed from the top view (Fig. 4h, i), the compacted
3 aggregates of granular K of sizes in the range of a few microns further confirms the
4 same finding, *i.e.*, a relatively flat and bulky K electrodeposits are generated. The
5 denser K deposition would lead to less exposure to the electrolyte, thus reducing the
6 detrimental decomposition reactions and improving battery cyclability. The foam-like
7 structures show distinct boundaries that are different from the previously scattered
8 dendrites. The currently observed foam-like structures may be formed due to repeated
9 stripping and plating of granular potassium (Fig. 4j). The corresponding 3D rendering
10 (Fig. 4k) provides a more direct and comprehensive picture of the distribution of the
11 compacted K deposition (yellow regions in Fig. 4k). Furthermore, the GF/D membrane
12 keeps its original state, and few "dead" K dendrites can be observed within. These
13 results clearly indicate that the Celgard 2400 separator possessing higher mechanical
14 integrity and strength could relatively suppress the growth of "dead" potassium
15 dendrites and enable reversible K plating/stripping.

16 The mechanism of the interaction between the K electrodeposits and the separators
17 is proposed in Fig. 5. During K electrodeposition (Fig. 5b), uneven K depositions
18 caused by nonuniform thickness and fragile tips can accelerate the K dendrite growth,
19 which could immensely disturb the distribution of the generated pressure. In the
20 meantime, the dendritic K electrodeposits with high activity would lead to continuous
21 dissolution and regeneration of SEI. During the extended electrochemical cycling, these
22 dendritic K electrodeposits could penetrate through the pores of the Celgard 2325,

1 accumulate within the locations between the tri-layers, stratify the separator and finally
2 propagate into the loose pores of GF/D membrane (Fig.5b), resulting in severe battery
3 polarization or short-circuit. Therefore, separators with loose pore structure are more
4 vulnerable to fail. In contrast, Celgard 2400 separators of high mechanical integrity and
5 bulk Young's modulus are desirable to facilitate compact K deposition to some extent
6 (Fig.5b). It is assumed that the dendrite-free potassium electrodeposits and self-
7 adaptable pressure originated from separators could significantly improve the
8 reversibility of K metal anodes. The self-adaptable pressure generated by high
9 mechanical separators would surpass the generation of dendritic K electrodeposits and
10 facilitate the formation of bulky-type K electrodeposition. These results suggest that
11 the intricate interplay between K electrodeposits and the separator critically affect the
12 cyclability and safety of KMBs.



14
15 Fig. 5. Schematic illustration of the morphology evolution of the separator during electrodeposition,

(a) A uniform K electrodeposition under a separator of ideal mechanical integrity. (b) An un-uniform K electrodeposition under separators of low/high mechanical integrity.

3. Conclusion

In summary, we have investigated the underlying interplay between the potassium electrodeposits and used separators by using customized tomography cells under various parameters, *i.e.*, electrolyte, depth of discharge, and cycling current density. Combining the *in-situ* visualizations of the customized tomography cells with the SEM analyses of the widely studied coin cells provides a reliable and comprehensive platform to assess the performance of the commercial separators. Our work highlights the importance of correlating electrochemical responses to the morphological changes of the electrode/separators. These results unambiguously demonstrate that the Celgard 2325 separator can be easily delaminated by the continuously growing and unevenly distributed K electrodeposits. In addition, the results also suggest that the loose space within the GF/D separator can function as a suitable "accommodation" for the accumulated K dendrites. In the last, the results imply that the Celgard 2400 separator which features relatively enhanced structural integrity and mechanical robustness can restrain the growth of K dendrites and maintain interfacial stability. To conclude, the direct visualization of the interplay of the interface chemistry and the K plating/stripping opens up new opportunities to understand the mechanism of the K deposition morphology. Combining such visualization technologies with other complementary techniques, such as *in-situ* TEM, cryo-EM, and FIB-SEM would be critical to further reveal the underlying mechanisms of nucleation and growth process

of K electrodeposits.

Appendix A. Supplementary information

Supplementary data associated with this paper about the experiment section and related details can be found online .

Author statement

Ling Ni: Formal analysis, Investigation, Writing - Original Draft **Markus Osenberg:** Software, Investigation, Visualization **Haijun Liu:** Formal analysis, Investigation **André Hilger:** Software, Formal analysis **Libao Chen:** Formal analysis, Writing - Review & Editing, Funding acquisition **Dong Zhou:** Formal analysis, Investigation **Kang Dong:** Formal analysis, Investigation **Tobias Arlt:** Software, Formal analysis, Investigation **Xiayin Yao:** Formal analysis, Writing - Review & Editing **Xiaogang Wang:** Resources, Formal analysis **Yanan Chen:** Formal analysis, Writing - Review & Editing **Yutao Li:** Formal analysis, Writing - Review & Editing **Kangning Zhao:** Formal analysis, Writing - Review & Editing **Chao Yang:** Formal analysis, Investigation, Writing - Review & Editing **Ingo Manke:** Formal analysis, Writing - Review & Editing **Fu Sun:** Formal analysis, Investigation, Writing - Review & Editing, Funding acquisition, Supervision **Renjie Chen:** Formal analysis, Writing - Review & Editing

Notes

The authors declare no competing financial interest.

Acknowledges

We acknowledge BESSY II for providing us valuable beam time. The work is supported by QIBEBT I201922, Dalian National Laboratory For Clean Energy (DNL) CAS, the China Scholarship Council (CSC), the National Natural Science Foundation of China (U1904216) and it is partially supported by the German Research Foundation, DFG (Project No. MA 5039/4-1).

References

1. B. Dunn, H. Kamath, J. Tarascon, Science 334 (2011) 928–935.

- 1 2. B. Kang, G. Ceder, *Nature* 458 (2009) 190–193.
- 2 3. W. Zhang, Y. Liu, Z. Guo, *Sci. Adv.* 5 (2019) 1–13.
- 3 4. K. Kubota, M. Dahbi, T. Hosaka, S. Kumakura, S. Komaba, *Chem. Rec.* 18 (2018) 1–22.
- 4 5. H. Liu, X. Cheng, Z. Jin, R. Zhang, G. Wang, L. Chen, Q. Liu, J. Huang, Q. Zhang, *Energy Chem*
- 5 1 (2019) 100003.
- 6 6. J. Ding, H. Zhang, W. Fan, C. Zhong, W. Hu, D. Mitlin, *Adv. Mater.* 32 (2020) 1908007.
- 7 7. X. Ren, Y. Wu, *J. Am. Chem. Soc.* 135 (2013) 2923–2926.
- 8 8. N. Xiao, X. Ren, W. McCulloch, G. Gourdin, Y. Wu, *Acc. Chem. Res.* 51 (2018) 2335–2343.
- 9 9. Q. Zhao, Y. Hu, K. Zhang, J. Chen, *Inorg. Chem.* 53 (2014) 9000–9005.
- 10 11. C. Zhang, J. Chen, X. Yin, Y. Sun, W. Yang, F. Yu, X. Liu, L. Fu, Y. Chen, Y. Wu DOI:
- 11 10.1039/d0cc06467j.
- 12 13. Y. Li, L. Zhang, S. Liu, X. Wang, D. Xie, X. Xia, C. Gu, J. Tu, *Nano Energy* 62 (2019) 367–375.
- 13 15. J. Hwang, S. Myung, Y. Sun, *Adv. Funct. Mater.* 28 (2018) 1802938.
- 14 16. Z. Wang, R. Pan, C. Ruan, K. Edström, M. Strømme, L. Nyholm, *Adv. Sci.* 5 (2018) 1700663.
- 15 17. W. Wang, F. Hao, P. Mukherjee, *ACS Appl. Mater. Interfaces* 12 (2020) 556–566.
- 16 18. J. Yan, F. Liu, Z. Hu, J. Gao, W. Zhou, H. Huo, J. Zhou, L. Li, *Nano Lett.* 20 (2020) 3798–3807.
- 17 19. D. Parikh, T. Christensen, C. Hsieh, J. Li, *J. Electrochem. Soc.* 166 (2019) A3377–A3383.
- 18 20. H. Liu, X. Gao, Y. Wang, T. Rojo, M. Armand, G. Wang, *Angew. Chem. Int. Ed.* 59 (2020)
- 19 16725–16734.
- 20 21. G. Cong, W. Wang, N. Lai, Z. Liang, Y. Lu, *Nat. Mater.* 18 (2019) 390–396.
- 21 26. P. Arora, Z. Zhang, *Chem. Rev.* 104 (2004) 4419–4462.
- 22 27. H. Zhang, M. Zhou, C. Lin, B. Zhu, *RSC Adv.* 5 (2015) 89848–89860.
- 23 28. Y. Liu, D. Yang, W. Yan, Q. Huang, Y. Zhu, L. Fu, Y. Wu, *iScience* 19 (2019) 316–325.
- 24 29. V. Deimede, C. Elmasides, *Energy Technology* 3 (2015) 453–468.
- 25 30. B. Wu, J. Lochala, T. Taverne, J. Xiao, *Nano Energy* 40 (2017) 34–41.
- 26 31. K. Chen, K. Wood, E. Kazyak, W. LePage, A. Davis, A. Sanchez, N. Dasgupta, *J. Mater. Chem.*
- 27 A 5 (2017) 11671–11681.
- 28 32. A. Sarkar, P. Shrotriya, A. Chandra, *J. Power Sources* 435 (2019) 226756.
- 29 33. P. Bai, J. Guo, M. Wang, A. Kushima, L. Su, J. Li, F. Brushett, M. Bazant, *Joule* 2 (2018) 2434–

1 2449.

2 34. Z. Ju, P. Li, G. Ma, Z. Xing, Q. Zhuang, Y. Qian, *Energy Storage Mater.* 11 (2018) 38–46.

3 35. Y. Chang, H. Sohn, *J. Electrochem. Soc.* 147 (2000) 50–58.

4 36. B. Song, I. Dhiman, J. Carothers, G. Veith, J. Liu, H. Bilheux, A. Huq, *ACS Energy Lett.* 4 (2019)

5 2402–2408.

6 37. E. Wang, C. Chiu, P. Chou, *J. Power Sources* 461 (2020) 228148.

7 38. L. Ding, D. Zhang, T. Wu, F. Yang, F. Lan, Y. Cao, M. Xiang, *Ind. Eng. Chem. Res.* 59 (2020)

8 4568–4579.

9 39. L. Zhang, T. Yang, C. Du, Q. Liu, Y. Tang, J. Zhao, B. Wang, T. Chen, Y. Sun, P. Jia, H. Li, L.

10 Geng, J. Chen, H. Ye, Z. Wang, Y. Li, H. Sun, X. Li, Q. Dai, Y. Tang, Q. Peng, T. Shen, S. Zhang,

11 T. Zhu, J. Huang, *Nat. Nanotechnol.* 15 (2020) 94–98.

12 40. Y. Hong, N. Lia, H. Chen, P. Wang, W. Song, D. Fang, D. Fang, *Energy Storage Mater.* 11 (2018)

13 118–126.

14 41. J. Park, J. Lee, M. Alfuruqi, W. Kwak, J. Kim, J. Hwang, *J. Mater. Chem. A* 8 (2020) 16718.

15 42. L. Wang, Z. Zhou, X. Yan, F. Hou, L. Wen, W. Luo, J. Liang, S. Dou, *Energy Storage Mater.* 14

16 (2018) 22–48.

17 43. H. Lu, X. Chen, Y. Jia, H. Chen, Y. Wang, X. Ai, H. Yang, Y. Cao, *Nano Energy* 64 (2019)

18 103903.

19 44. X. Zhang, E. Sahraei, K. Wang, *Sci. Rep.* 6 (2016) 32578.

20 45. L. Francine, Z. Raphael, W. Vanessa, *J. Electrochem. Soc.* 165 (2018) A1829–A1836.

21 46. D. Finegan, S. Cooper, B. Tjaden, O. Taiwo, J. Gelb, G. Hinds, D. Brett, P. Shearing, *J. Power*

22 *Sources* 333 (2016) 184–192.

1
2
3
4
5
6



7
8
9
10
11
12
13

Ling Ni received his B.S. degree from Taiyuan University of Technology (China) in 2013, and earned Ph.D. degree from the School of Chemistry at Jilin University in 2019 under the supervision of Prof. Zongtao Zhang. Dr. Ni is now pursuing his postdoctoral training with Prof. Dingguo Xia at Qing Dao Institute of Bioenergy and Bioprocess Technology, Chinese Academy of Sciences. Her current research focuses on potassium metal batteries.



14
15
16
17
18
19

Markus Osenberg studied Physics at Technical University Berlin (TUB), Germany. From 2012 to 2016, he worked as a student associate at Helmholtz-Zentrum Berlin (HZB), Germany. Since 2016, he has been working as a PhD student at HZB analyzing novel battery materials by X-ray, ion and electron imaging and machine learning techniques.



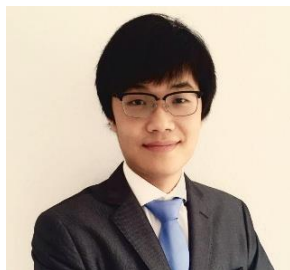
1
2 **Haijun Liu** received his M.Sc. degree from China University of Petroleum in 2019. During 2019
3 and 2020, she worked at the Qingdao Institute of Bioenergy and Bioprocess Technology, Chinese
4 Academy of Sciences as a research assistant. She is now a Ph.D. candidate in China University of
5 Petroleum. Her research interests include the design, synthesis and characterization of advanced
6 energy materials for Li/Na-ion batteries.
7



8
9 **Dr.-Ing. André Hilger** is responsible for the synchrotron and neutron tomography facilities and the
10 3D data analysis center at the Helmholtz-Zentrum Berlin (HZB), Germany. He studied Technical
11 Physics at the University of Applied Science (TFH) Berlin, Germany. After receiving his diploma
12 degree he worked as a technician at HZB as well as at TFH between 2001 and 2006. In 2006, he
13 obtained his MEng degree from TFH. In 2009, he completed his PhD thesis in materials science.
14 Up to now, he is a post-doc at HZB in the field of imaging techniques for energy research.
15



1 **Prof. Libao Chen** received his B.S. degree and M.S. degree from Central South University in 2001
2 and 2004 and Ph.D. degree from the Shanghai Institute of Microsystem and Information Technology,
3 Chinese Academy of Sciences in 2007. He is now a professor in the State Key Laboratory of Power
4 Metallurgy at Central South University. His main research interest is focused on the high-
5 performance energy storage materials and devices, including Li alloy anode, Zinc anode, lithium
6 ion batteries and lithium sulfur batteries.



8
9 **Dong Zhou** received his PhD in Materials Science from Technical University of Berlin, Germany
10 in 2017, and worked as a research scientist at MEET Battery Research Center, University of
11 Muenster from September 2017 to June 2019. Since July 2019, he joined Ningbo Institute of
12 Materials Technology & Engineering (NIMTE), Chinese Academy of Sciences as an Assistant
13 Professor. His research activities are focused on electrochemical kinetics and charge compensation
14 mechanism studies in rechargeable batteries.



16
17 **Dr. Kang Dong** is currently a post-doc at Helmholtz-Zentrum Berlin. He obtained his PhD degree
18 at Technical University Berlin (TUB) under the supervision of Dr. Ingo Manke and Prof. John
19 Banhart. His work is focused on X-ray and electron based characterization and the degradation
20 mechanism of electrode materials for lithium and sodium batteries.



Dr. Tobias Arlt studied physics at the TU Berlin from 2001 to 2008 and wrote his diploma thesis at the Ferdinand-Braun-Institut in Berlin. There he investigated ohmic contacts on gallium nitride-based semiconductor materials. From 2009 to 2012 he received his PhD at the Helmholtz-Zentrum Berlin in the Institute for Applied Materials Research in the field of imaging techniques for fuel cell research. Since then he has been developing radiographic and tomographic measurement methods for X-rays analysis. Current fields of interest are battery, fuel cell and electrolyzer research as well as biological and cultural topics.



Dr. Xiayin Yao is a professor at Ningbo Institute of Materials Technology and Engineering, Chinese Academy of Sciences (NIMTE, CAS). He received Ph.D from Institute of Solid State Physics and NIMTE, CAS in 2009. After that, he joined NIMTE and worked there until now. He worked as a research fellow or visiting scholar in Hanyang University, S. Korea (2012-2013), Nanyang Technological University, Singapore (2013-2014) and University of Maryland, College Park, USA, (2018-2019). His major interests include all-solid-state lithium/sodium batteries.



Xiaogang Wang is an associate professor in Qingdao Institute of Bioenergy and Bioprocess Technology (QIBEBT), Chinese Academy of Sciences (CAS). He earned his PhD from Changchun Institute of Applied Chemistry (CIAC), CAS (2009) in Physical Chemistry. After a postdoctoral fellow at the University of Texas at Austin and Michigan State University, he joined QIBEBT in 2011. His current research focuses on the design and controllable preparation of advanced functional materials for the applications in the energy conversion and storage device, such as alkali metal batteries, lithium ion batteries, electrochemical supercapacitors and polymer electrolyte membrane fuel cells.



Yanan Chen is a professor in School of Materials Science and Engineering, Tianjin University. He received his joint Ph.D. from University of Science and Technology Beijing/University of Maryland in 2017. He was an advanced innovative fellow at Tsinghua University before joining in Tianjin University. His research mainly focuses on nanomaterials, devices, and systems for advanced energy storage and conversion. His research interests include nanomaterials synthesis and nanomanufacturing; emerging energy storages Li-ion and beyond; catalysis; Cryo-EM.



Yutao Li is a research fellow at the University of Texas at Austin in United States. He received his Ph.D. degree in Materials Science and Engineering from Tsinghua University in 2013. Now he is working with Prof. John B. Goodenough to do the research work about transitional metal oxides and their application in batteries and catalysts.



Kangning Zhao is currently PostDoc of the Laboratory of Advanced Separations (LAS) at the School of Basic Science, École Polytechnique Fédérale de Lausanne (EPFL). He received his Ph.D. degree from Wuhan University of Technology in 2019, during which, he carried out his visiting scholar research in the laboratory of Prof. Xudong Wang at the University of Wisconsin-Madison in 2016–2018. Currently, his research interest includes membranes for electrochemical catalysis and energy storage devices.



Chao Yang received his M.Sc. degree from Hainan University in 2018. During 2016 and 2018, he studied at Peking University as a joint M.Sc. student. He is now a Ph.D. candidate in Technische Universität Berlin. His research interests include the design, synthesis and characterization of advanced energy materials for Li/Na/K-ion batteries, solid-state electrolyte and catalysis.

1



2

3 **Dr. Ingo Manke** is head of the “Imaging Group” at the Helmholtz-Zentrum Berlin für Materialien
4 und Energie (HZB) and reader at the Technical University Berlin (TUB). He studied Physics at the
5 Freie Universität Berlin and received a PhD in Solid State Physics from TUB in 2002. His research
6 area focuses on the development of imaging techniques based on X-rays, neutrons and electrons and
7 on their application on energy-related materials.

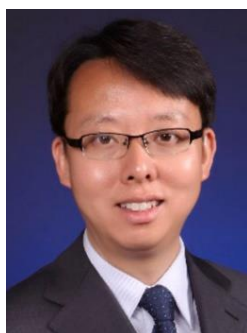
8



9

10 **Dr. Fu Sun** has received his Ph.D. degree from Technical University of Berlin in 2017. Afterwards,
11 Dr. Sun has been working as a postdoctoral fellow at Helmholtz Zentrum Berlin für Materialien und
12 Energie for the following 2 years. He is now currently a senior research fellow at Qingdao Institute
13 of Bioenergy and Bioprocess Technology, Chinese Academy of Sciences. His research interest is
14 focused on investigating working mechanisms and/or failure modes of various types of rechargeable
15 batteries by non-destructive synchrotron X-ray and neutron imaging techniques.

16



17

18 **Renjie Chen** is a Professor in the School of Materials Science and Engineering at Beijing Institute
19 of Technology (BIT). His research focuses on electrochemical energy storage and conversion
20 technology. He was a post-doctoral fellow in Department of Chemistry at Tsinghua University and
21 a visiting professor in Department of Materials Science and Metallurgy at University of Cambridge.
22 As the principal investigator, Prof. Chen successfully hosted the National Key Research and
23 Development Program of China, National Natural Science Foundation of China, and National High

1 Tech. 863 project *etc.* He (co-) authored ~286 research papers and filed 88 patents and patent
2 applications.
3